CHAPTER 3

GRAVITY DATA AND DATA REDUCTION

3.1 Data coverage

The gravity data used in this study were obtained by using the automated gravity meter, Scintrex CG-3 (serial No. 101175). A total of 532 data points carried out along the accessible paths and tracks with 0.2 km intervals are covered an area as shown in Figure 3.1. The instrument yields a reading directly in milligal (mGal) and a reading at each station can be stored in its internal memory. In this study, only one reference station (base station) was used in reoccupation of each traverse after finishing each survey. This procedure was done to manipulate short term instrument drift caused by both transportation and handling.

The measurement at a set of stations are repeated at base station at interval of 5 to 6 hr. The Autograv gravimeter does not only allowing the user to apply a real date and time for surveying but also automatically calculates a tidal correction to each reading by selecting the automatically tidal correction feature. The reading time was 120 seconds and repeated measurements were made at some stations where the measurements were taken on unstable ground or the measurements were operated under windy conditions. An overall accuracy better than $\pm$ 0.02 mGal for gravity anomalies and $\pm$ 5 cm for the elevation were measured.

As stated in chapter 1, it should be evident that horizontally adjacent strata with contrasting densities is the necessary configuration to produce a gravity anomaly. However, there are some peripheral surface

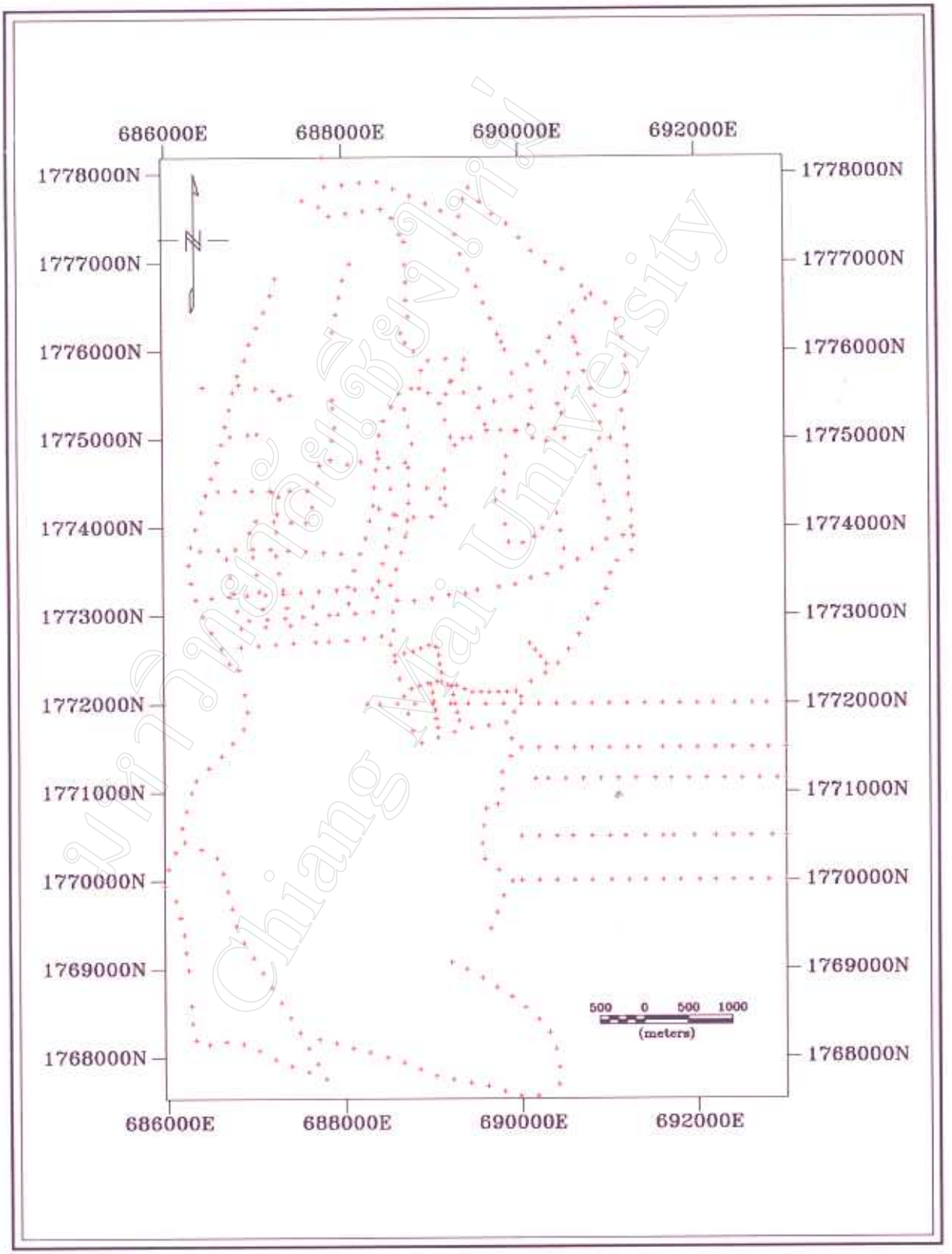

Figure 3.1 Location of gravity data collection.

influences that can obscure the true subsurface gravity values. Therefore, it is necessary to eliminate these effects by correction observed gravity values reducing to the values they would have on a datum equipotential surface. The process is known as gravity data reduction and base station level is the standard datum level in this study.

3.2 Gravity data reduction

An anomaly value at a point on the earth is equal to the observed gravity value minus a predicted gravity value based on a given earth model or the anomaly is the difference between what is measured and what is predicted. Six correction factors which are frequency concerned to bring about the gravity anomalies are drift correction, tidal correction, latitude correction, free-air correction, bouguer correction, and terrain correction. These are known as the gravity reduction procedures. In this study, the procedures for reduction are processed by the GRAVRED computer program. This program is part of the Geosoft geoscientific data processing and presentation package (Geosoft, 1994).

Data processing procedures are illustrated in Figure 3.2. The instrument gravity reading of all traverses are firstly dumped into a microcomputer for further processing purposes. With the instrument dump facility, a new file format with *dmp* extension is created automatically. The station number 9999, either positive or negative, is used to indicate base station. Subsequently, this *dmp* file will be convert to geosoft GRAVRED file format to get another new file format with extension *raw* (Appendix A). At this state, both elevation and

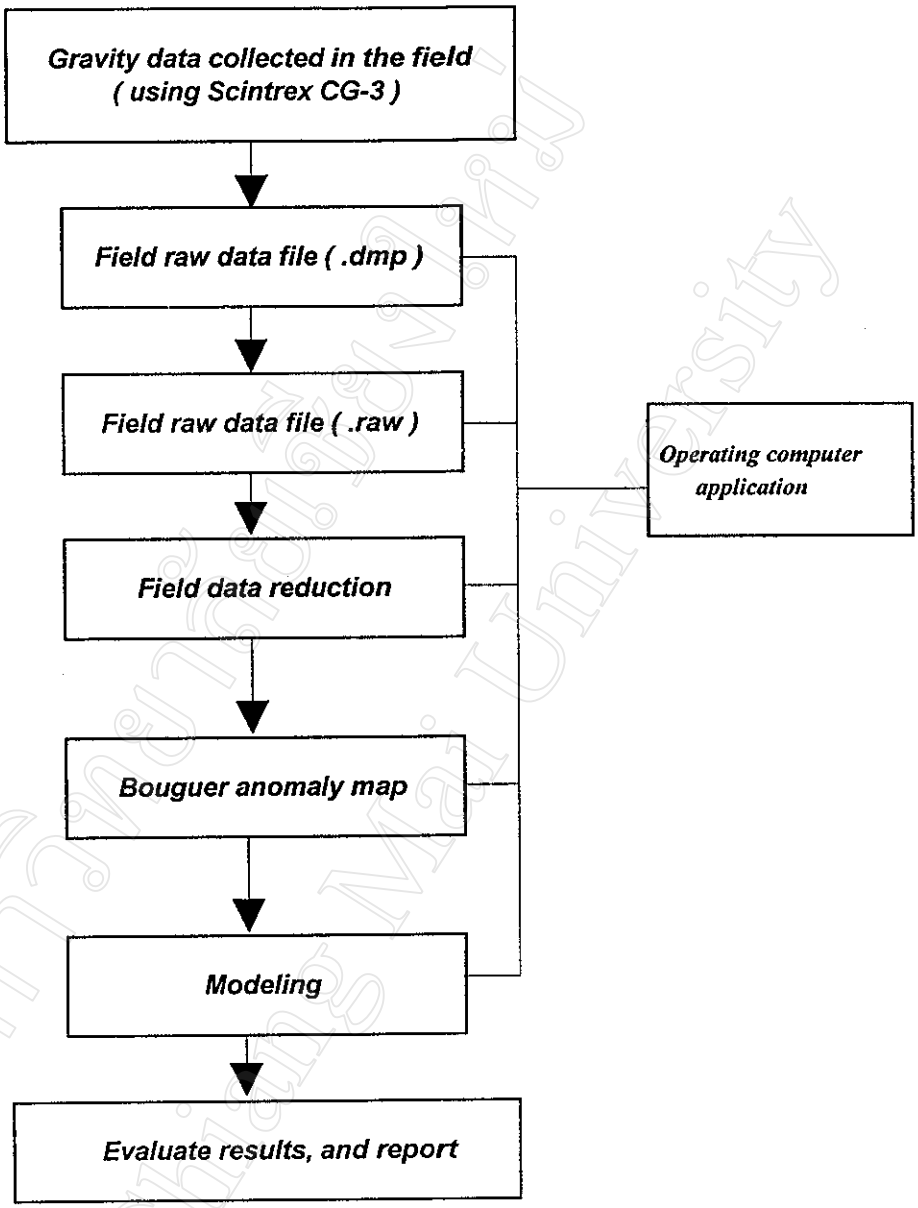

Figure 3.2 Schematic illustrations of procedures for data processing

geographic location at each station are called for completed *raw* file format (Table 3.1 and 3.2).

Consequently, this raw data will be applied to the standard gravity data reductions of GRAVRED computer program. The input requirement for GRAVRED program are; survey date, GMT time difference, bouguer density, the coordinate projection or UTM zone number (UTM 47), and International Gravity Formula of 1967. Having these parameters, the program reduces the data for all gravity data reductions, except terrain correction, and yield both free-air anomaly and bouguer anomaly.

Although the study area has small isolated hills, e.g., Khao Thep Phanom and Khao Cha-Ngok, located along the eastern limit of the study area, and Khao Khan Tha around the NW portion of the map, but corrections values are negligible comparing with gravity reading. Low topographical relief at each station affect the corrections varying from 0.004 to 0.03 mGal. For example, as noted on Table 3.3, the terrain corrections are applied at each point along the line No. 34. This N-S trending line is carried out near Khao Khan Tha. The corrections have been calculated to a distance on a map of about 2,600 m (bounding zone I of Hammer's chart) and these values make terrain correction negligible. The common equation using to reduce gravity data to get the complete value of bouguer anomaly is given by

$$g_B = g_{obs} \pm \left(\Delta g_L \pm \Delta g_{FA} \mp \Delta g_B + \Delta g_T\right) \qquad (3.1)$$

where g_B is the value of the bouguer anomaly for the station, g_{obs} is the station reading which includs both drift and tidal corrections, and the rest of the symbols in bracket are the corrections that mentioned before.

Table 3.1 Example of *raw* file format

Job:1. Grid:1. Line:34.N Oper:1. CG3#:101175.

dt=94/03/10 gm= -7

Stn	X	Y	Time	Rdng	In_Ht	Elev
-9999	*	*	09:58:04	163.559	16.0	57.936
9	*	*	11:47:04	165.213	61.0	*
7	*	*	11:50:28	165.213	60.0	*
5	*	*	11:54:46	165.184	61.0	*
3	*	*	11:59:04	165.025	60.0	*
1	*	*	12:03:10	164.857	60.0	*
-9999	*	*	13:36:32	163.583	16.0	57.936

Table 3.2 Example of completed *raw* file format

Job:1. Grid:1. Line:34.N Oper:1. CG3#:101175.

dt=94/03/10 gm= -7

Stn	X	Y	Time	Rdng	In_Ht	Elev
-9999	*	*	09:58:04	163.559	16.0	57.936
9	687889	1776211	11:47:04	165.213	61.0	62.787
7	687929	1776408	11:50:28	165.213	60.0	64.196
5	687965	1776603	11:54:46	165.184	61.0	65.767
3	688009	1776798	11:59:04	165.025	60.0	66.883
1	688090	1776981	12:03:10	164.857	60.0	67.463
-9999	*	*	13:36:32	163.583	16.0	57.936

Table 3.3 Example of terrain correction values along line No. 32

Station No.	X (m)	Y (m)	Elevation (m)	Bouguer (mGal)	T (mGal)	Abs-Bouguer (mGal)
1	687889	1776211	62.8	3.59	0.023	3.613
2	687929	1776408	64.2	3.78	0.027	3.807
3	687965	1776603	65.8	3.98	0.025	4.005
4	688009	1776798	66.9	3.95	0.027	3.977
5	688090	1776981	67.5	3.82	0.029	3.849

Noted: T=Terrain correction.

According to sprase sampling of gravity data, the data sets obtained from GRAVRED program are then transformed to an equally grid using a Random Gridding program of Geosoft. The process of Geosoft Random Gridding Program interpolates the readings to determine the values at the nodes of a grid by fitting a two-dimensional surface based on a minimum-curvature method.

The program first estimates grid values at the nodes of a coarse grid based on the inverse distance average of the actual data within a specified search radius. It usually uses grid cell size about ¼ of the map scale. If there is no data within that radius, the average of all data points in the grid is used. An iterative method is then employed to adjust the grid to fit the actual data points nearest the coarse grid nodes. Once an acceptable fit is achieved, the coarse cell size is divided by 2 and the same process repeated using the coarse grid as the starting surface.

This is repeated until the minimum curvature surface is fit at the final grid cell size. A contour map was produced from this initial grid using a MAPPLOT program that using a spline under tension techniques for a slight smoothing of the contours as shown in Figure 3.3 and Figure 3.4, the free-air gravity anomaly map and the bouguer anomaly map respectively.

3.3 Data enhancement

In order to offer the opportunities to develop many of derived maps for further interpretation, data enhancement techniques are considered to separate the bouguer anomaly into two constituent parts,

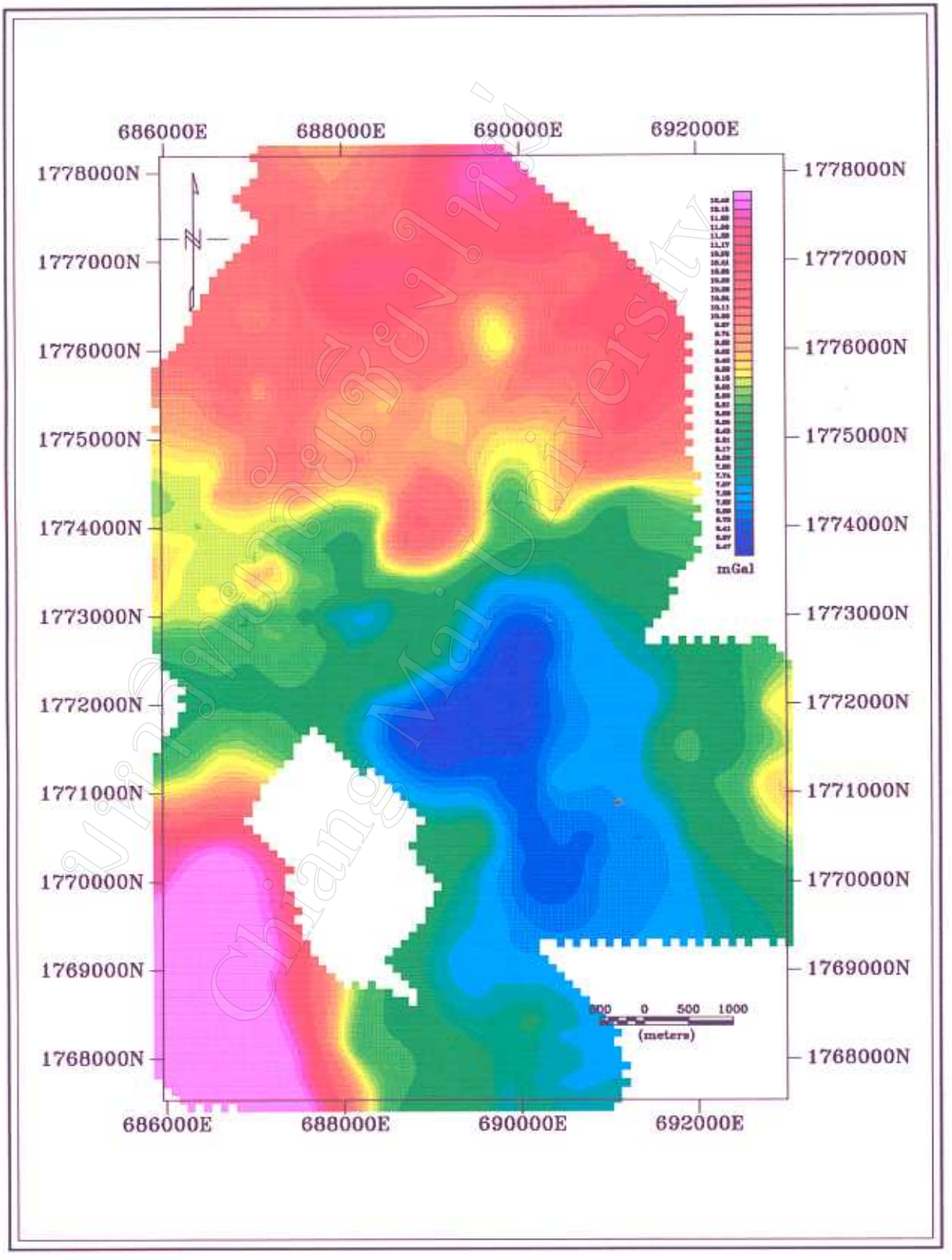

Figure 3.3 Free-air anomaly map

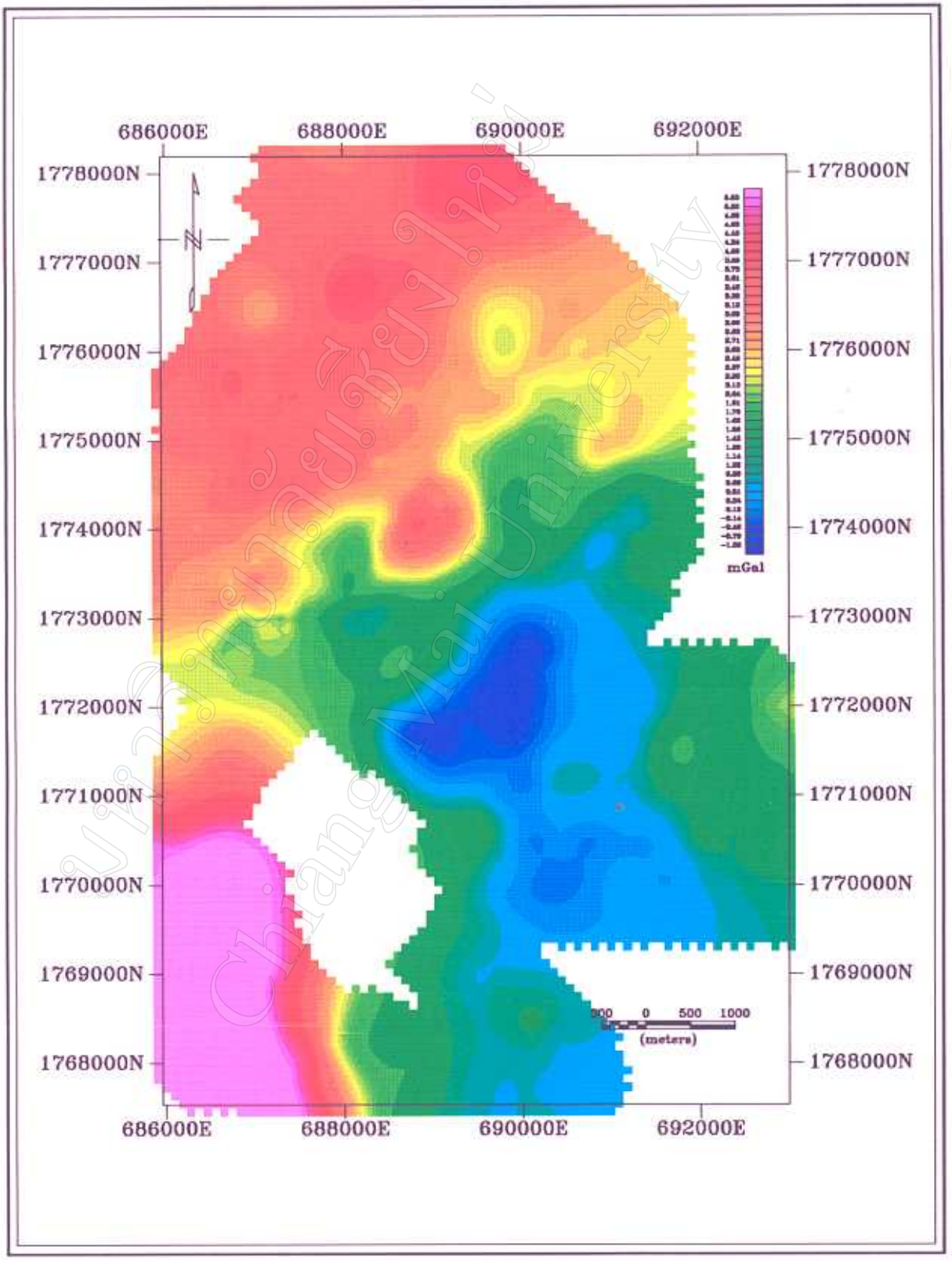

Figure 3.4 Bouguer anomaly map

i.e. the regional and residual component (Nettleton, 1954, Swartz, 1954, and Agarwal and Sivaji, 1992). To enhance the gravity data, the space domain bouguer gravity data were transformed into frequency domain using the MAGMAP Fast Fourier Transformation (FFT) computer algorithm of the Geosoft software package.

A number of computer programs in the MAGMAP has the facilities to apply different data enhancement techniques. The techniques which are applied in this study are low pass filtering, upward continuation, band pass filtering, and second vertical derivative filter, respectively. Then, results of each were then transformed back to space domain to get the enhanced gravity anomaly maps.

3.4 Qualitative interpretation

Both free-air and bouguer anomaly map reveals two spatially characteristic patterns. These patterns are distinguished on the basis of contour lines and amplitudes of the anomalies. The main pattern reflects the broad gradient which decreases in gravity across the study area with NW-SE trending. It is generally accepted that the gradients probably indicate underlying fault zones (Kane, and Godson, 1985). The other anomaly pattern is reflected by the prominent SW-NE trending, the high positive anomaly and its characteristic with dome shape at the northern portion of the map and the negative anomaly with blue color zone at the center of the map.

Recall from chapter 1 that the positive anomaly is the one that would be expected in this study. Then, the distinctive area which high positive anomaly is expected to be anhydrite mass underlying gypsum

ores deposited. It is assumed that the observed anomalies are the resultant of the individual effects of bodies of comparable sizes lying at different depths, the spectral characteristics of the anomalies can be used as a discriminating parameter for sources at different depths.

The first step should be the determination of the frequency intervals where the energy of the spectrum is concentrated. The aim of this step is to identify whether measurable anomalies related to source at the desired depth exist and to choose the cut off frequency for the low pass filters which are prepared to get rid of contributions due to shallow bodies. The parameter for filtering are introduced from Figure 3.5. Noted on that Figure, the spectrum composes of four major components; noise component (between C and D), shallowest component (between B and C), shallow component (between A and B), and deep component (less than A). By choosing the parameters of 3.1 cycle/km, 1.2 cycle/km, and 0.41 cycle/km respectively, the filtered maps were then produced.

In an attempt to isolate the near-surface horizon, the deep source can be displayed by choosing upward continuation and low pass filter techniques. The upward continuation of about 1,000 m in Figure 3.6 reveal the point that as the high frequency is eliminated and the height of upward contribution increase, the near surface are attenuated and only the deep features are retained. It also should be noticed that the underlying component of the field shows a NNE-SSW strike, possible swinging to NNW-SSE in the SW portion of the map. Figure 3.7 shows the resulting after filtering with the low pass filter. This filter rejects the component of the spectrum with frequencies greater than 0.41 cycle/km. The anomalies due to the deep horizon are running in a NE-SW direction which is similar to the pattern in Figure 3.6.

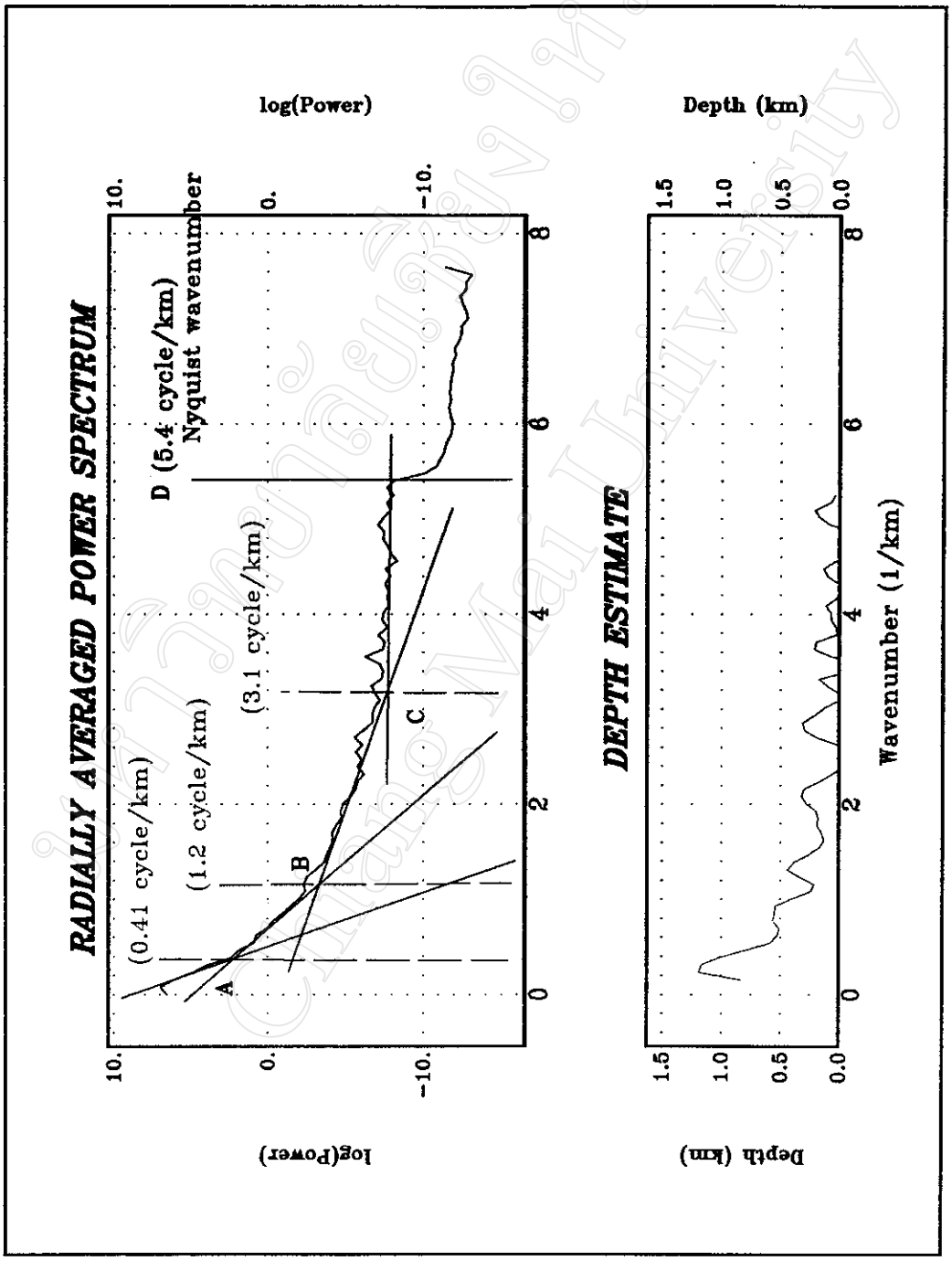

Figure 3.5 Gravity power spectrum.

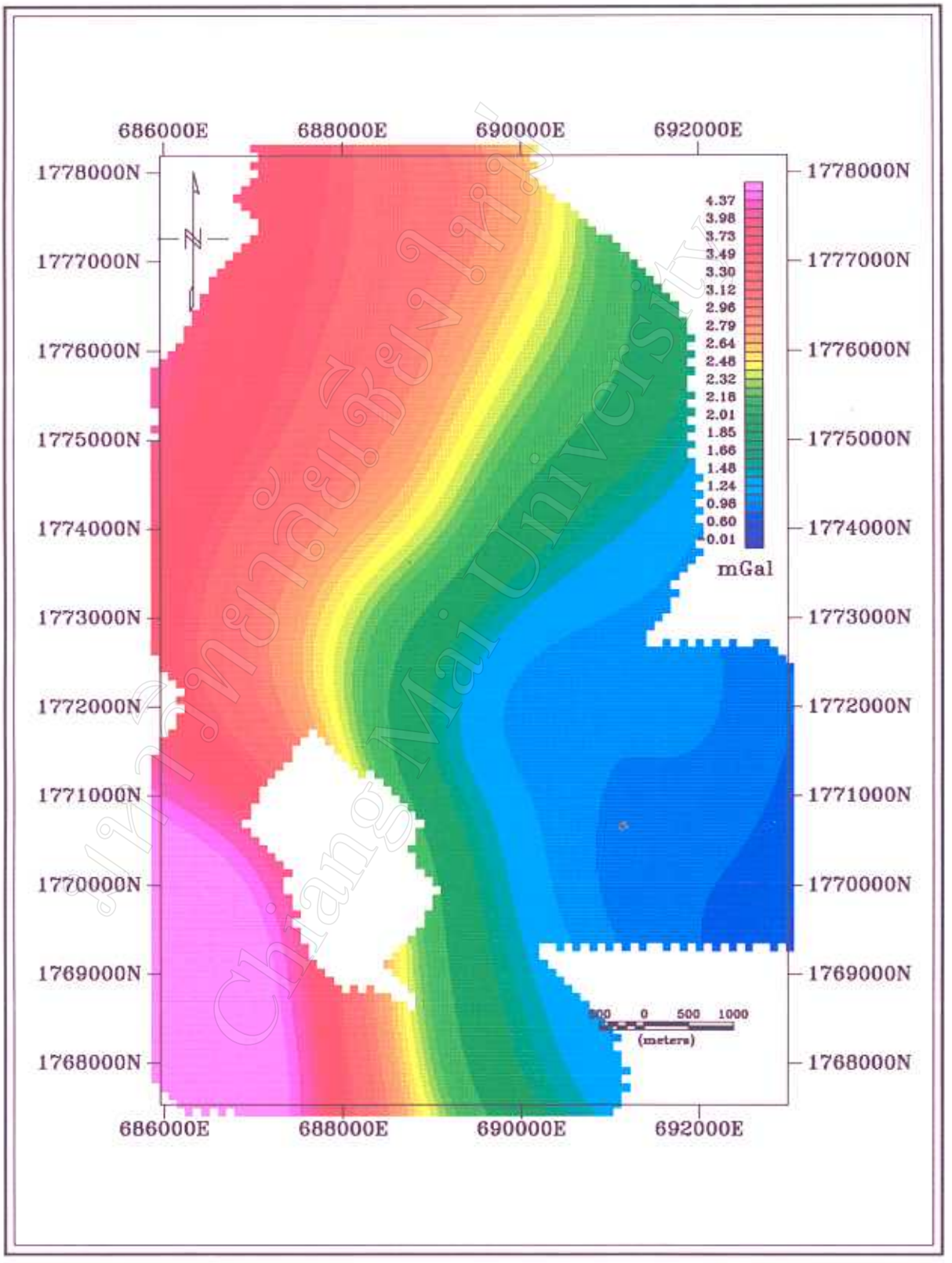

Figure 3.6 The bouguer anomaly map after applying upward continuation technique to an elevation of +1,000 m.

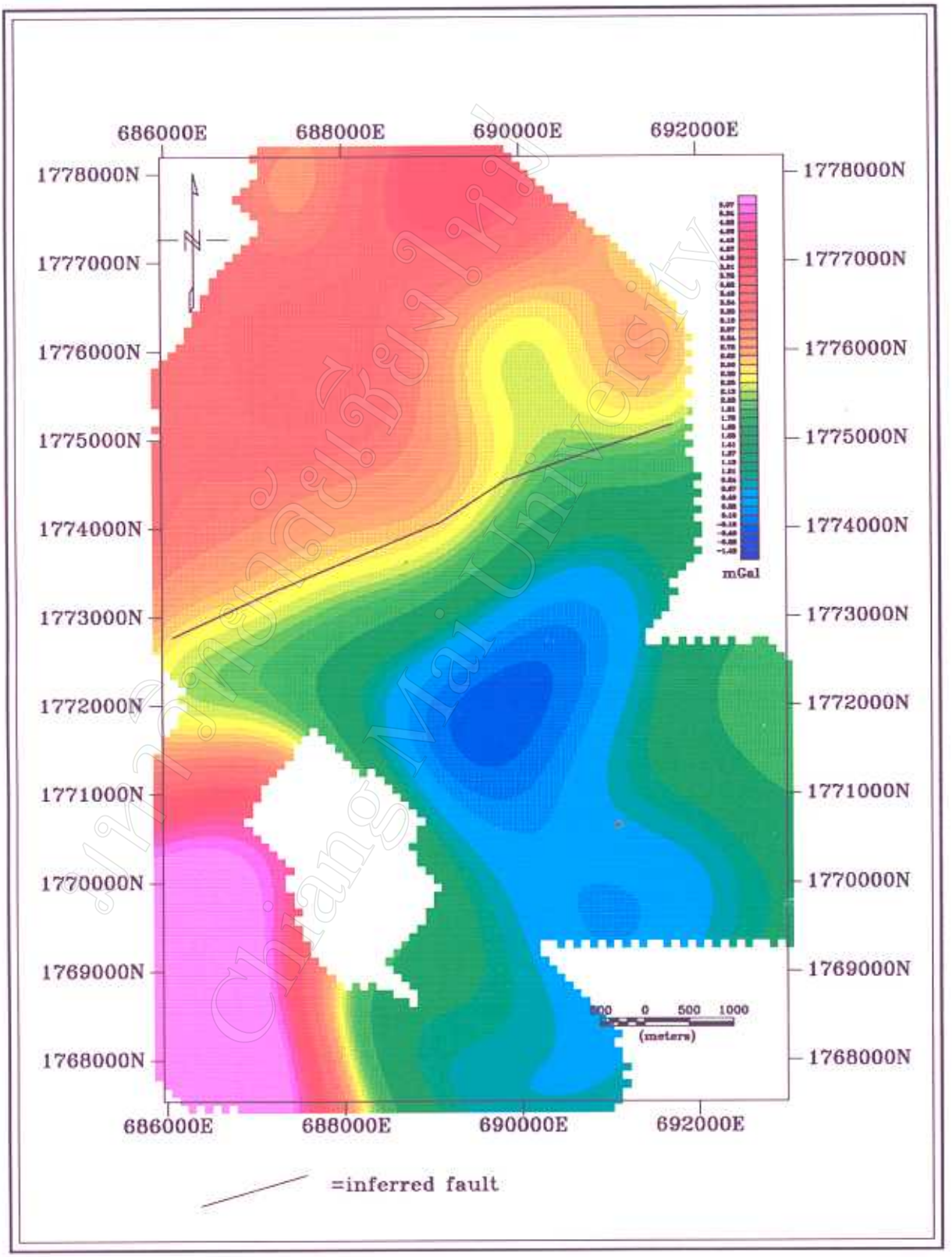

Figure 3.7 The bouguer anomaly map after applying low pass filter with wavenumber less than 0.41 cycle/km

Figure 3.8 shows the results when apply a band pass filter that passes frequencies between 0.41 cycle/km and 3.1 cycle/km. Note that most of the energy due to the deep sources and high frequency noise component has been removed. The remaining energy results mainly from the field due to the shallow and not so deep sources. The anomalies on the filtered map indicate the same presence and position of the NE-SW trending.

Considering the second vertical derivative in Figure 3.9, the prominent anomalies pattern is also running in NE-SW direction. This techniques is useful in isolating the anomalies and obtained by differentiating the potential in various ways. Noted on that figure, the anomaly patterns are similar to that one in Figure 3.8. Then, as indicated in the filtered maps, the prominent feature in the study area having a NE-SW strike is probably be fault. This feature confirms with an inferred fault from geological map of the study area.

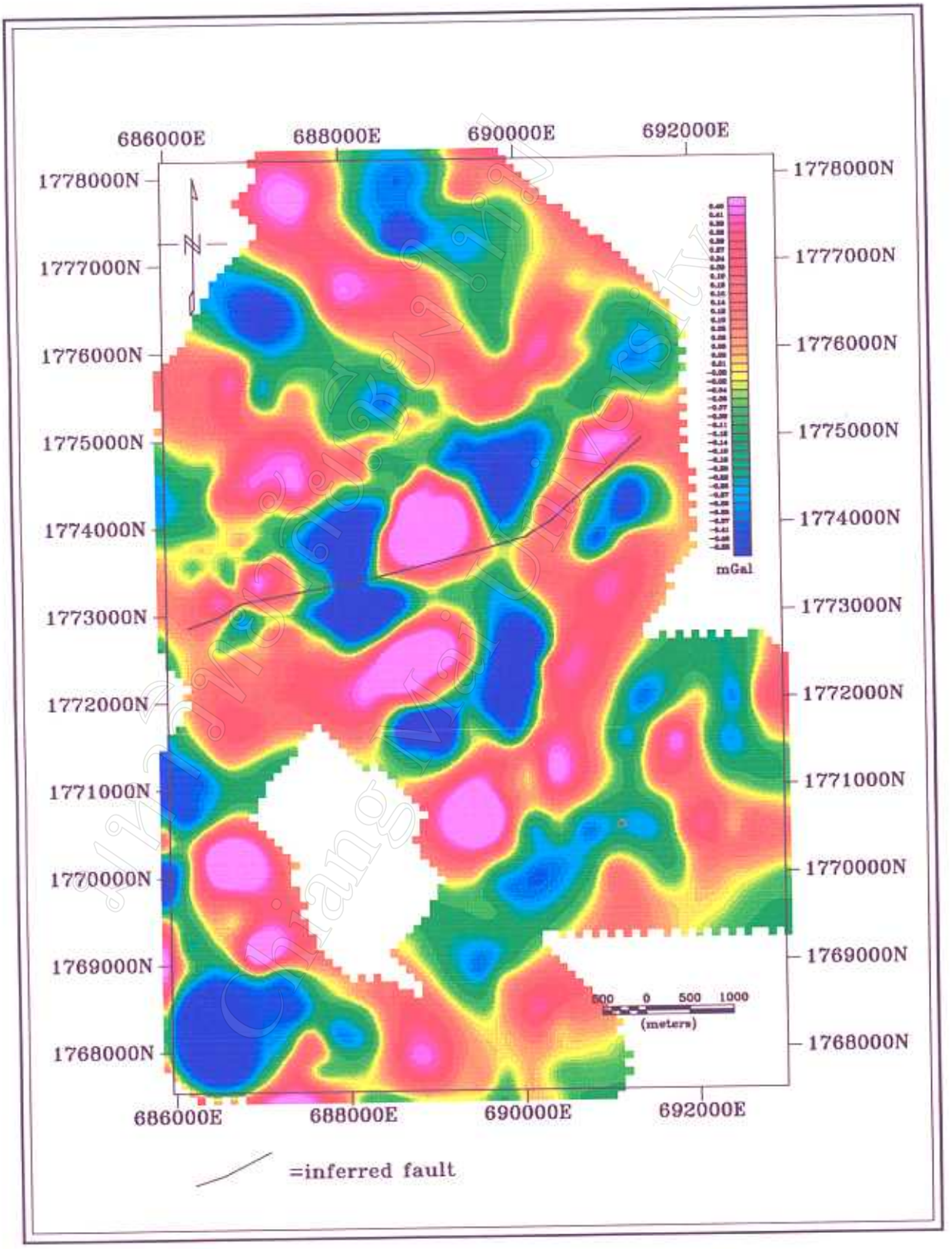

Figure 3.8 The bouguer anomaly map after applying band pass filter with wavenumber between 0.41 cycle/km and 3.1 cycle/km

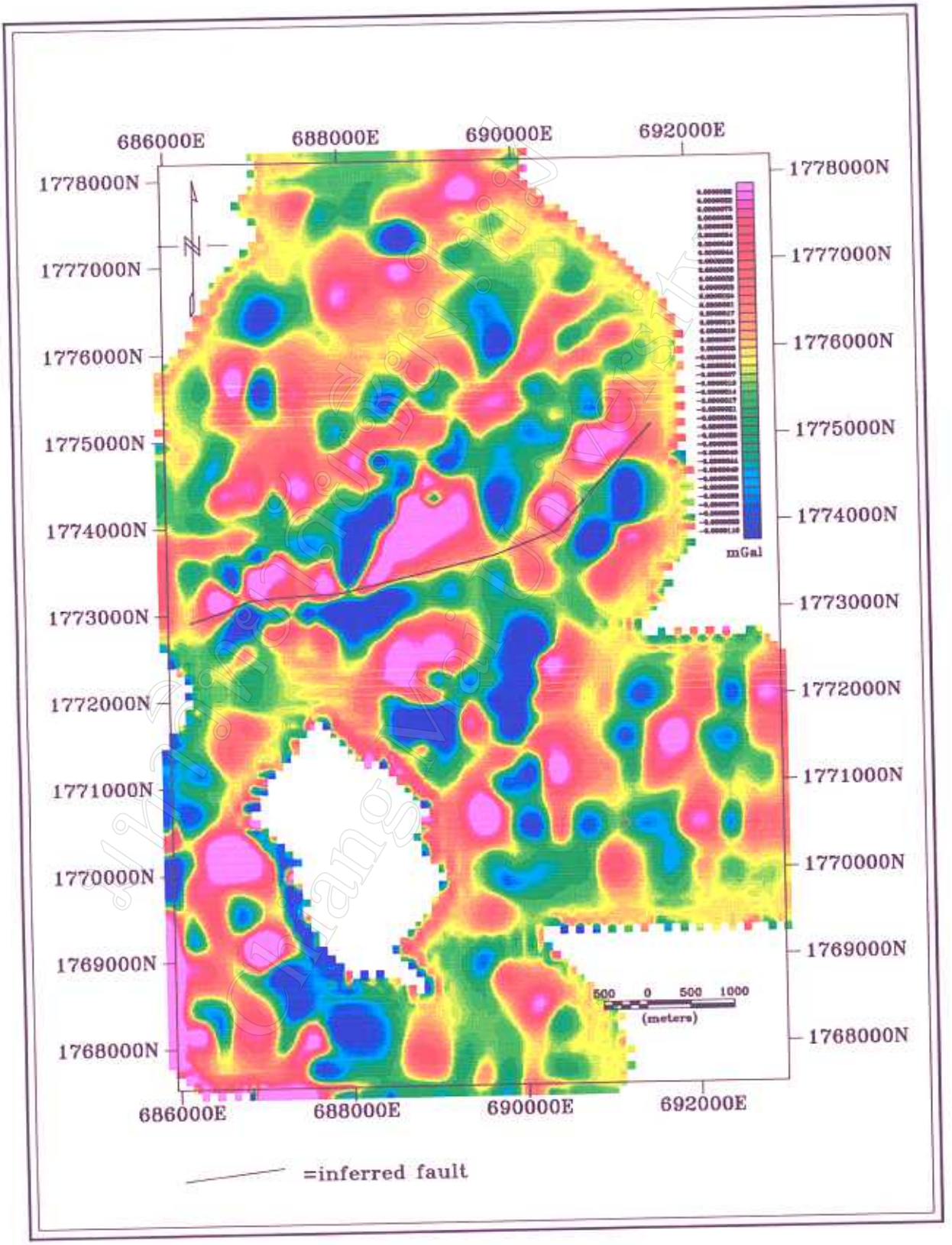

Figure 3.9 The bouguer anomaly map after applying second order vertical derivative filter.